


RESEARCH ARTICLE

Open Access



SIRPα antibody combined with oncolytic virus OH2 protects against tumours by activating innate immunity and reprogramming the tumour immune microenvironment

Defeng Kong¹, Zhenrong Yang¹, Guoliang Li¹, Quanyou Wu¹, Zhaoru Gu¹, Duo Wan¹, Qi Zhang¹, Xiaoli Zhang¹, Shujun Cheng¹, Binlei Liu^{2*}, Kaitai Zhang^{1*} and Wen Zhang^{3*} 

Abstract

Background: The combination of oncolytic viruses (OVs) with immune checkpoint blockades is a research hotspot and has shown good efficacy. Here, we present the first attempt to combine oncolytic herpes simplex virus 2 (OH2) with an anti-SIRPα antibody as an antitumour treatment. Our results provide unique insight into the combination of innate immunity with OV.

Methods: We verified the polarization and activation of OH2 in RAW264.7 cells in vitro. Subsequently, we evaluated the antitumour ability of OH2 and anti-SIRPα combined therapy in a tumour-bearing mouse model. RNA-seq and Single-cell RNA-seq were used to characterize the changes in the tumour microenvironment.

Results: The OH2 lysates effectively stimulated RAW264.7 cells to polarize towards the M1 but not the M2 phenotype and activated the function of the M1 phenotype in vitro. In the macrophage clearance experiment, OH2 therapy induced polarization of M1 macrophages and participated in the antitumour immune response in a tumour-bearing mouse model. Treatment with a combination of OH2 and anti-SIRPα effectively inhibited tumour growth and significantly prolonged the survival time of the mice, and this result was more obvious in the mouse model with a larger

*Correspondence: liubl@hbut.edu.cn; zhangkt@cicams.ac.cn; zhangwen@cicams.ac.cn

¹ State Key Laboratory of Molecular Oncology, Department of Etiology and Carcinogenesis, National Cancer Center/National Clinical Research Center for Cancer/Cancer Hospital, Chinese Academy of Medical Sciences and Peking Union Medical College, Beijing 100021, China

² National "111" Center for Cellular Regulation and Molecular Pharmaceutics, Key Laboratory of Fermentation Engineering (Ministry of Education), Hubei Provincial Cooperative Innovation Center of Industrial Fermentation, College of Bioengineering, Hubei University of Technology, Wuhan 430068, China

³ Department of Immunology, National Cancer Center/National Clinical Research Center for Cancer/Cancer Hospital, Chinese Academy of Medical Sciences and Peking Union Medical College, Beijing 100021, China



tumour volume at the beginning of the treatment. These results suggest that combination therapy can more profoundly reshape the TME and activate stronger innate and adaptive immune responses.

Conclusions: Our data support the feasibility of oncolytic virus therapy in combination with anti-SIRP α antibodies and suggest a new strategy for oncolytic virus therapy.

Keywords: Oncolytic virus, Oncolytic herpes simplex virus 2, SIRP α , Macrophage, Tumour microenvironment environment

Background

The use of viruses for cancer therapy began more than a century ago. With the development of genetic engineering and advances in the understanding of the mechanism of action of viruses, oncolytic viruses (OVs) may become an ideal therapeutic platform. An increasing number of studies have shown that the killing effect of OVs on tumour cells is not only via direct cytolytic activity but also involves a complex regulatory mode combining multiple mechanisms [1]. These mechanisms include regulating changes in the tumour micro- and macroenvironment, specific immune responses mediated by CD8+ T cells, and innate immune cellular immune responses [2–4]. Despite their multiple mechanisms of therapeutic activity, many preclinical and clinical studies have shown that most oncolytic viruses, whether armed or unarmed, show limited efficacy as monotherapies [5, 6]. The ability of oncolytic viruses to modify the tumour microenvironment (TME) and alter immunologically "cold" tumours suggests that a combination of oncolytic viruses with other therapies, such as immunotherapy or chemotherapy, may achieve better therapeutic outcomes [7, 8].

At present, combining OVs and immune checkpoint blockade (ICB) is a research hotspot and has shown good efficacy in some clinical trials [9]. However, the combination of OVs and immunotherapy mainly focuses on the regulation of T cells, and there are few studies on its effect on innate immunity. OVs promote immunogenic cell death (ICD) during cell lysis, thereby recruiting and activating innate immune cells such as macrophages and dendritic cells through the release of damage-associated molecular patterns (DAMPs) and pathogen-associated molecular patterns (PAMPs) and further promoting the activation of tumour-specific T cells in the TME [4, 10]. Therefore, the activation of myeloid cells to activate tumour killing and enhance antigen presentation to activate endogenous immune function is expected to provide unique insights for antitumour therapy.

Macrophages are a class of highly plastic immune cells with a variety of functions that are usually divided into classically activated M1 macrophages and M2 macrophages based on their polarization state [11]. M1 macrophages promote the inflammatory Th1 response through the release of inflammatory cytokines and

further enhance the T cell response through upregulation of antigen presentation and the expression of costimulatory molecules [11, 12]. Therefore, M1 macrophages may be involved in antitumour immunity in the tumour microenvironment. M2 macrophages are generally associated with the inhibition of endogenous antitumour immunity. Reducing the number of M2 macrophages and increasing the number of M1 macrophages are important prerequisites for successful tumour therapy. In addition, the phagocytic function of macrophages is regulated by the CD47-SIRP α antiphagocytic axis [13]. CD47 inhibits phagocytosis of macrophages through high expression on tumour cells [13, 14]. Anti-phagocytosis of the CD47-SIRP α axis can be blocked by antibodies, thus increasing the phagocytosis of macrophages. A recent study showed that blocking SIRP α on macrophages can effectively activate the antitumour ability of macrophages [15].

In previous studies [16, 17], we found that treatment with oncolytic herpes simplex virus 2 (OH2) can effectively alter the TME and induce an antitumour immune response in mice. In this study, we treated a mouse tumour model with a combination of OH2 and an anti-SIRP α antibody. We analysed the therapeutic effect and immune activation status of combination therapy. Our results suggest OH2 combined with the activation of macrophages is a promising antitumour therapy.

Methods

Cell line and oncolytic virus

The CT26, MC38, 4T-1, and RAW264.7 cell lines were purchased from the National Infrastructure of Cell Line Resource (Beijing, China) and kept by our laboratory. The cells were cultured in a constant temperature incubator containing 5% CO₂ at 37°C.

OH2 was provided by Binhui Biopharmaceutical Co., Ltd. (Wuhan, China). The virus was an attenuated OH2 derived from the wild-type HSV-2 strain HG52 deleted the ICP47 gene and ICP34.5 gene [18, 19].

Lysate preparation

The CT26, MC38, and 4T-1 cell lines in the logarithmic growth phase were passaged to 10 cm² culture dishes when the cells reach 70–80% confluence, rinse the cells with PBS and then add 5 ml serum-free RPMI-1640

medium (HyClone, Waltham, MA) and infect the cells with OH2 according to $MOI=1$, and add 5 ml RPMI1640 medium containing 10% FBS (Gibco, Waltham, MA) after 1 h. After 30 h, the cell supernatant was collected, centrifuged at 4°C, 400 g for 5 min, and the lysate was collected and stored at -80°C for later use. The cell-free supernatant (CFS) of CT26, 4T-1, MC38, and untreated RAW264.7 were used as control. The CFS of CT26, 4T-1, and MC38 was obtained from the culture supernatant of cells in a logarithmic growth phase, centrifuged at 4°C, 400g for 5 min. The supernatant of CT26, MC38, and 4T1 cell lysate prepared by repeated freezing and thawing was also used as the control group.

Cell viability test

RAW264.7 cells in the logarithmic growth phase were spread on a 96-well plate at 2000 cells/well and cultured for more than 6 h. After the cells adhered, added the lysate and controls were added to the cells, and Cell Counting Kit-8 (CCK8) detection was performed at the corresponding time points (0 h, 6 h, 12 h, 24 h, 48 h) (Dojindo, Kumamoto, Japan). Before detection, 100 µl of detection working solution (CCK8 reagent: RPMI1640 medium = 1:10) was added to each well and incubated for 1 h in a 37°C, 5% CO₂ incubator in the dark. Finally, a microplate reader (Bio-Rad, Japan) was used to detect the absorbance of the cells at a wavelength of 450 nm.

Flow cytometry to detect the polarization direction of macrophages

RAW264.7 cells in the logarithmic growth phase were spread to a 6-well plate at 10⁶ cells/well. After at least 6 h, the cells were completely attached to the wall, and the lysate and control were added separately. After 24 h of treatment, RAW264.7 cells were stained with FITC anti-mouse F4/80 (clone: FJK-16s, Invitrogen, Waltham, Massachusetts), APC anti-mouse CD86 (clone: GL-1, Biolegend, San Diego, CA) and PE anti-mouse CD206 (clone: MR6F3, Invitrogen, Waltham, Massachusetts) according to the protocol of the antibodies (M1 macrophage: F4/80+CD86+, M2 macrophage: F4/80+CD206+) and subjected to flow cytometry (LSR II, BD). Detection of SIRPα on macrophages in spleen from mouse used FITC anti-mouse F4/80, APC anti-mouse CD11b (clone: M1/70, Biolegend, San Diego, CA), and PE anti-mouse SIRPα (clone: P84, Biolegend, San Diego, CA). All flow cytometry used to detect macrophage typing in this study was set up with an antibody isotype control group (PE Rat IgG2a, clone: RTK2758, Biolegend, USA; APC Rat IgG2a, clone: RTK2758, Biolegend, USA; FITC Rat IgG2a, clone: RTK2758, Biolegend, USA).

Functional experiments on macrophages

The CT26, MC38, and 4T-1 cell lines in the logarithmic growth phase were digested and resuspended at a concentration of 1×10⁶/mL. One µL of CFSE (C34554, Life Technology, Waltham, MA) working solution (0.5 mM) was added to every 2ml of tumour cells with a concentration of 1×10⁶/mL and incubated at 37°C (5% CO₂) for 8 min. After the incubation, 10ml of pre-cooled RPMI 1640 medium containing 10% FBS was added to stop staining. The supernatant was discarded by centrifugation, and the cell concentration was adjusted to 5×10⁵/mL with RPMI 1640 medium with 10% FBS. The concentration of raw264.7 treated with lysate and control was adjusted to 5×10⁶/mL. With the ratio of 25:1, 50:1, and 100:1 as the effector to target ratio parallel samples, co-cultivation was carried out in a 96-well U-shaped well plate, 100µL raw264.7 cells, and 100µL tumour cells were added to each well, and 3 parallel samples were set up. Then placed the culture plate a 37°C (5% CO₂) for 4 h. Before testing, 200 µL of PI (P8080, Solarbio, Beijing, China) working solution (2.5µg/mL) was added to each culture well.

Detection of the expression level of CD47 and SIRPα in vivo and in vitro

The CT26, MC38, and 4T-1 cell lines and macrophages in the spleen of mice were stained with APC anti-mouse CD47 (clone: miap301, Biolegend, San Diego, CA), purified anti-mouse SIRPα (clone: P84, Biolegend, San Diego, CA) and anti-mouse IgG-Alexa 488 (ab150113, Abcam, Cambridge, UK) antibodies according to the protocol of the antibodies. The expression levels of CD47 and SIRPα were detected by flow cytometry.

Immunohistochemical staining

The paraffin-embedded tissue sections were baked at 60–65°C for more than 6 h and then put in xylene for dewaxing while hot. Steps were followed by gradient ethanol hydration, citrate repair antigen (ZLI 9064, Zsjiqbio, Beijing, China), 3% hydrogen peroxide blocking endogenous peroxidase activity, blocking (SP-KIT-B2, MXB, Fujian, China), primary antibody F480 (clone: SP115, dilution: 1:200, Abcam, Cambridge, UK), CD86 (clone: E5 W6H, dilution: 1:500, CST, Danvers, Massachusetts), CD206 (polyclonal, dilution: 1:100, Abcam, Cambridge, UK), CD8 (polyclonal, dilution: 1:200, Affinity Biosciences, Jiangsu, China), CD16 (polyclonal, dilution: 1:200, Affinity Biosciences, Jiangsu, China) and horseradish peroxidase (HRP)-conjugated secondary antibody (Kit-5010, MXB, Fujian, China) incubation, visualized with the 3,30-diaminobenzidine DAB (DAB-1031, MXB, Fujian, China) chromogen, haematoxylin staining (Solarbio, Beijing, China), hydrochloric acid ethanol differentiation, and ammonia

water returning to blue. Finally, after dehydration with gradient ethanol, tissue sections were dehydrated in xylene and sealed with neutral gum. After drying, tissue sections were observed for staining under a microscope (Nikon Eclipse 80i, Japan).

Multicolour immunohistochemical staining

The paraffin-embedded tissue sections were baked at 60°C–65°C for more than 6 h and then put in xylene for dewaxing while hot. After gradient ethanol hydration and neutral formalin immersion, each stained antibody was sequentially repaired by citrate, blocked by goat serum, and incubated with primary antibodies against F480 (clone: SP115, dilution: 1:500, Abcam, Cambridge, UK), CD86 (clone: E5 W6H, dilution: 1:1000, CST, Danvers, Massachusetts), CD206 (polyclonal, dilution: 1:200, Abcam, Cambridge, UK), CD8 (polyclonal, dilution: 1:500, Affinity Biosciences, Jiangsu, China), CD16 (polyclonal, dilution: 1:500, Affinity Biosciences, Jiangsu, China) and secondary antibody, and fluorescently stained to amplify the signal. After the staining was completed, the DAPI working solution was added dropwise, and finally, the super anti-quenching mounting tablet was added to the mount as required by the instructions in the kit (TSA-RM, PANOVIEW, Beijing, China). The stained tissue slices were scanned and analysed with Plaris and Inform software.

IHC images were scanned using CaseViewer2.4 software. The degree of staining was scored: cells with staining <10% were scored as negative staining (–, 1), cells with staining 10–49% were scored as (+, 2); cells with staining rate of 50–74% were scored as (++,3), 75–100% stained cells were denoted as (+++, 4). Staining positive range scores are as follows: colourless (0); pale yellow particles (1), tan particles (2), and brown particles (3). The final score was defined as the staining extent score multiplied by the staining positive range score [20]. Negative expression scores ranged from 0 to 5, with positive expression scores over 5 [21].

Animal model construction

The mice were purchased from Beijing Vital River Laboratory Animal Technology Co., Ltd. (Beijing Vital River Laboratory Animal Technology Co., Ltd.). Six- to 8-week-old female Balb/c mice weighing approximately 19–20 g were kept in a laminar flow ultraclean rack in our animal room under specific aseptic conditions for approximately 1 week. Each mouse was inoculated subcutaneously (s.c.) with 3×10^5 CT26 cells on the right side of the dorsal area. The tumour appeared in approximately 5–7 days, and treatment was given when the diameter of the tumour grew to 3–5 mm or 8–10 mm.

All operations were carried out under the standard operating procedures of the specific pathogen-free (SPF) experimental mouse breeding management system specified by the state. All animal-related experimental procedures were approved by the Committee on the Ethics of Animal Experiments of the National Cancer Center/Cancer Hospital, Chinese Academy of Medical Sciences (CAMS), and Peking Union Medical College.

The first part

CT26 cell subcutaneous transplantation tumour model was constructed. When the diameter of the tumour reached 3–5 mm (day 7), the mice in the CL model were separated into three groups (OH2 [OH2 + Control Liposomes], OH2 + CL, and PBS control group) with an even distribution of tumour volumes. Assigned more than 10 mice to each group. OH2 (2×10^6 plaque-forming units [PFU]) was performed by intratumoural injection (i.t.) on day 0, day 2, and day 4 in a volume of 100 μ l. One hundred microliters of CL (7 mg/mL, F70101C-NC, FormuMax, Sunnyvale, CA) or control liposomes (7 mg/mL, F70101-N, FormuMax, Sunnyvale, CA) per mouse was given by intraperitoneal injection (i.p.) at the day before the OH2 treatment. The PBS control group was given 100 μ L PBS per mouse. Tumour growth was regularly observed and recorded for each group of mice. After 14 days of treatment, the tumour tissues were resected for immunohistochemical and multicolour immunohistochemical staining. The mice in the survival observation group were tumour-bearing again on the 40th day.

The second part

A CT26 cell subcutaneous transplantation tumour model was constructed. When the diameter of the tumour reached 3–5 mm (day 7), it was defined as the tumour being smaller at the time of initial treatment. The mice in the anti-SIRP α model with smaller tumours at initial treatment were separated into six groups (OH2 + anti-SIRP α antibody group, OH2+isotype group, OH2 group, anti-SIRP α antibody group, isotype group, and PBS control group) with an even distribution of tumour volumes. Assigned more than 10 mice to each group. The OH2 treatment or PBS was injected on days 0, day 2, and day 4, and the anti-SIRP α antibody (clone: P84, Bioxcell, Lebanon, New Hampshire) or isotype (TNP6A7, Bioxcell, Lebanon, New Hampshire) was administered on days 1 and 3. The anti-SIRP α antibody and isotype were injected intraperitoneally (i.p.) with 100 μ g, diluted to 1 mg/ml with PBS without preservation solution, and injected 100 μ L intraperitoneally for each mouse. The PBS control group was given 100 μ L PBS per mouse. The administration method and dosage of the OH2 were the same as

those in the CL model. The tumour growth of mice was observed and recorded regularly every two days.

When the diameter of the tumour reached 8–10 mm (day 14), it was defined as the tumour being larger at the time of initial treatment. The mice in the anti-SIRP α model with larger tumours at initial treatment were separated into four groups (OH2+ anti-SIRP α antibody group, OH2+isotype group, OH2 group, anti-SIRP α antibody group, and PBS control group) with an even distribution of tumour volumes. Assigned more than 10 mice to each group. The mode of administration and treatment strategy was the same as described above. The tumour growth of mice was observed and recorded regularly. After 12 days of treatment, the tumour tissues were resected for immunohistochemical, multicolour immunohistochemical staining, and RNA sequencing.

When the experimental endpoint or humanitarian endpoint was reached, such as when the size of the mouse reached 2500 mm³ or tumour metastasis or rapid growth caused ulceration, necrosis, or infection that interfered with eating or walking, the mice were anaesthetized with 5% chloral hydrate and then sacrificed by cervical dislocation. The calculation formula of tumour volume was $\text{volume} = (\text{length} \times \text{width}^2) / 2$.

RNA sequencing

The transcriptome sequencing involved in this study was undertaken and completed by Tianjin Nuohe Zhiyuan Bioinformation Technology Co., Ltd. RNA samples were required to reach a total volume of ≥ 30 μL , a total volume of ≥ 1.5 μg , and a concentration of ≥ 50 ng/ μL . The agarose gel electrophoresis quantification method, Nanodrop, and Agilent 2100 were used to test the concentration, purity, and integrity of the submitted RNA. The type of library construction was a eukaryotic chain-specific library. The sequencing strategy was Illumina HiSeq-PE150 (two-way sequencing).

Single-cell RNA sequencing

The tumour tissues of the control group, OH2 group, and combined treatment group were subjected to single-cell sequencing analysis, and the single-cell sequencing technology used in this study was provided by Huada Company. The tissue was dissociated using the Tumor Dissociation Kit (mouse, MACS), the dead cells were removed, and the single-cell suspension of living cells was left for sequencing. The data obtained were analysed using the Seurat package, and the volcano plot was drawn using the R software package Enhanced-Volcano. The R packages used for GO analysis and KEGG analysis included tidyverse, patchwork, monocle, clusterProfiler, org.Mm.eg.db.

Bioinformatics analysis

R software version 4.0.2 was used to analyse the transcriptome sequencing data, and the R software package “edgeR” was used for differential expression analysis between groups. Gene set enrichment analysis (GSEA) was used to study the difference signal pathways between different groups. The R software package “clusterProfiler” was used for Gene Ontology (GO) and Kyoto Encyclopedia of Genes and Genomes (KEGG) analysis. Gene set variation analysis (GSVA) was used for immune cell infiltration analysis. Student’s *t*-test was used to compare the differentially expressed genes, and the *P*-value was adjusted and corrected by the Benjamini-Hochberg method. The log₂-fold-change was greater than 1, and the corrected *P*-value was less than 0.01 as the threshold to judge the significance of the difference. A total of 770 immunology-related mouse genes created from the nCounter Mouse PanCancer Immune Profiling Panel (NanoString) were used as reference genes which are listed in Additional file 1: Table S1 and Additional file 2: Table S2.

Statistical analysis

GraphPad Prism software version 8 was used for statistical analysis and statistically significant differences were defined as a *p* value < 0.05. Two-tailed, unpaired Student’s *t*-test was used to compare two groups. Two-way analysis of variance (ANOVA) was performed on the experimental data for tumour volumes for more than two groups. The Kaplan-Meier method and log-rank test were used for the survival curve data; the survival period was defined as the time from the start of treatment to the end of the observation. The results are presented as the mean \pm S.E.M. In this study, all experiments were repeated at least three times, except for the parts otherwise stated.

Results

OH2 lysates could induce macrophage polarization and activation in vitro

We confirmed the role of macrophages in the process of OH2 treatment of colon cancer, as shown in Fig. 1A. As shown in Fig. 1B, the RAW264.7 cells treated with the lysates had significantly enhanced viability and proliferation ability by CCK8 assay ($p < 0.0001$ for CT26 and MC38 cells, $p = 0.001$ and $p < 0.0001$ compared with the cell-free supernatant (CFS) and untreated RAW264.7 and 4T-1 cells, respectively). The lysates stimulated the activation of macrophages. We also incubated OH2 at different MOIs (MOI=1, MOI=0.5) with RAW264.7 cells to determine whether OH could directly activate macrophages through CCK8. As expected, the addition

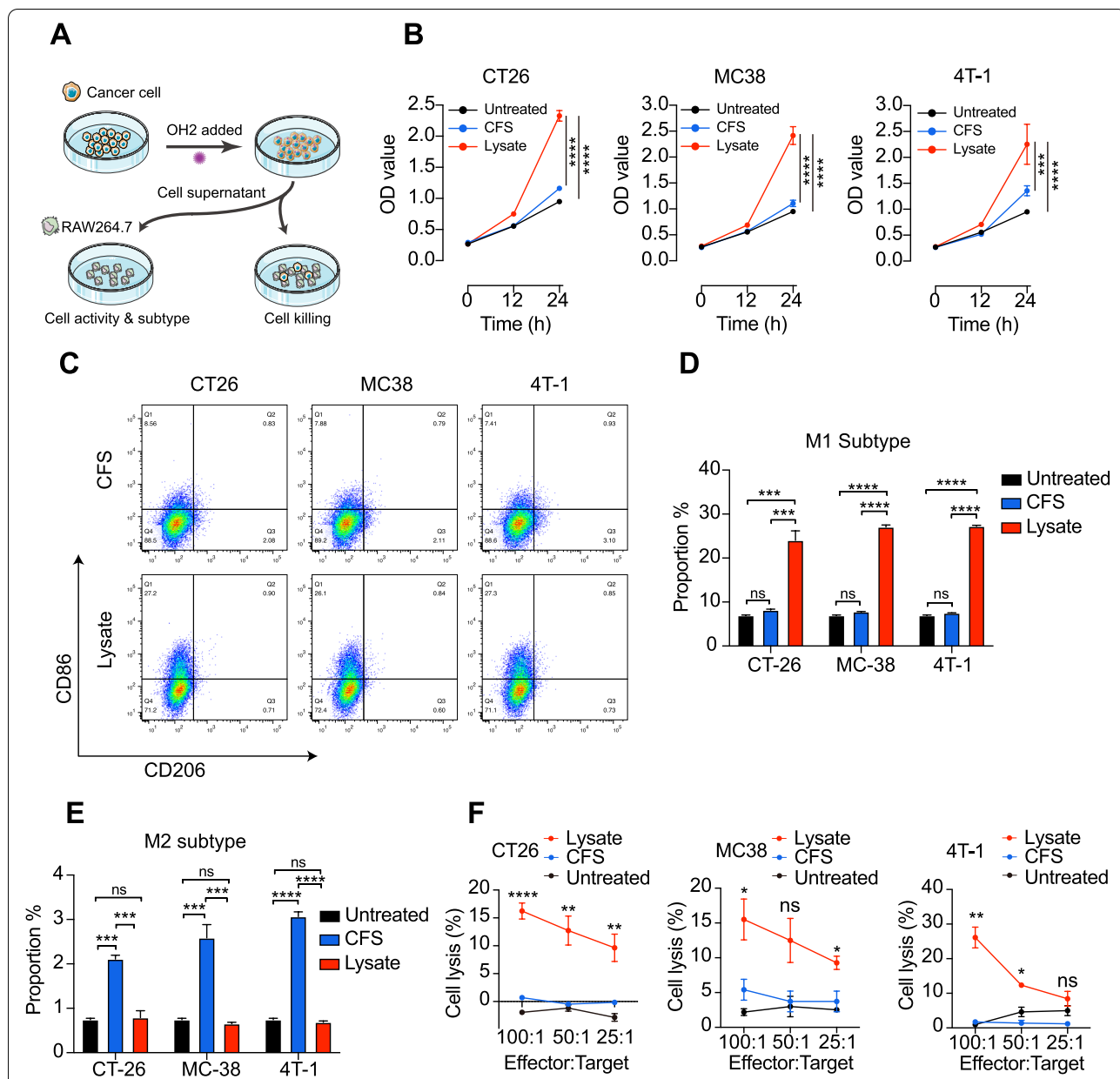
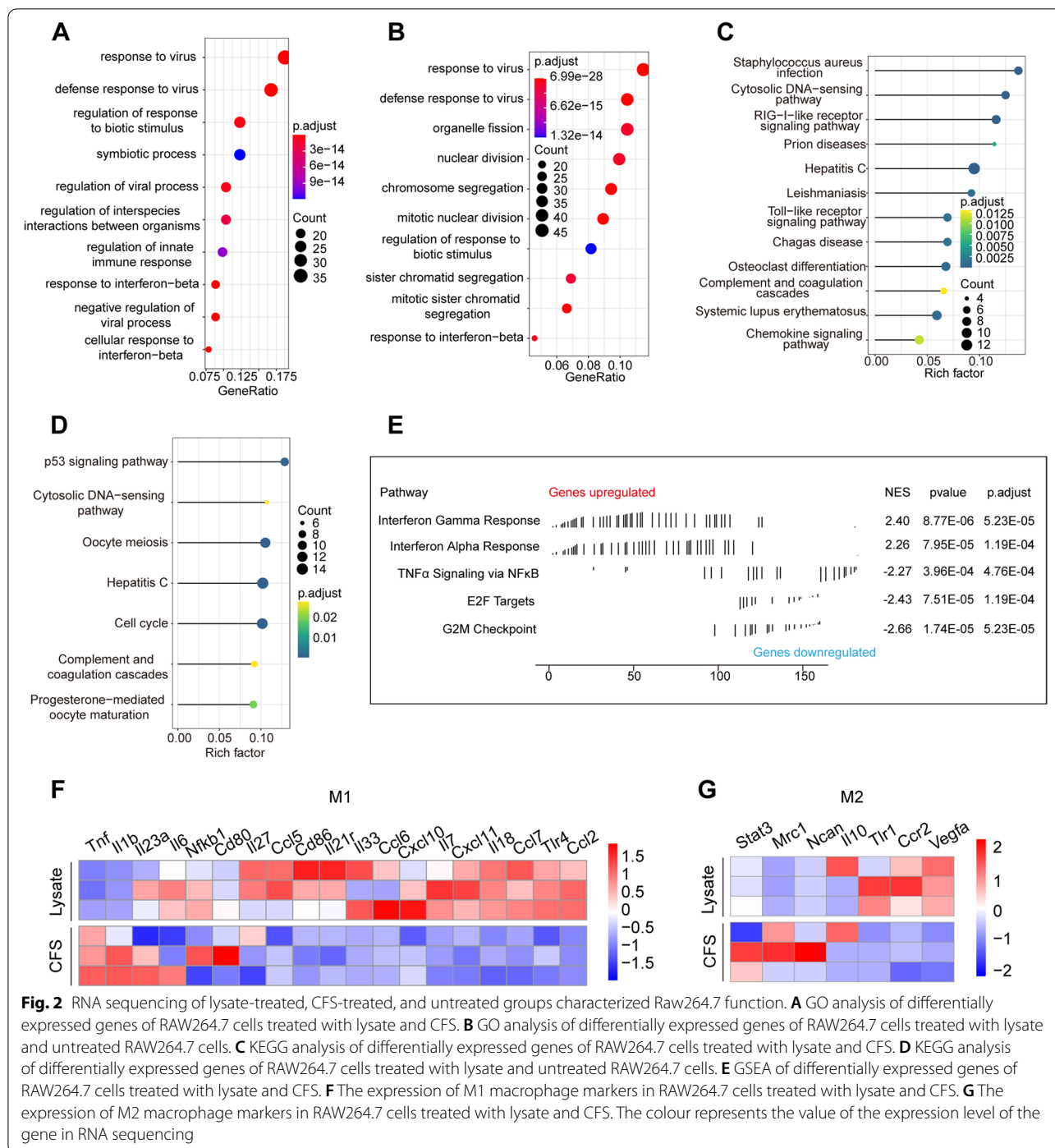


Fig. 1 OH2 lysates induce RAW264.7 polarization and phagocytosis in vitro. **A** Schematic of lysate preparation and flowchart of the experiment performed in the study. **B** Cell proliferation assay results of CT26 (left), MC38 (middle), and 4T-1 (right) cell lines treated with lysate (red), CFS (blue), and untreated (black) group by CCK8 assay in 24 h. **C** Flow cytometric analysis results of one representative sample from each cell line with lysate or CFS treatment. **D** The percentage of M1 (F4/80+CD86+) subtype in the lysate, CFS, and untreated groups of CT26, MC38, and 4T-1 cells detected by flow cytometry. The data are averages from three samples per treatment group. An unpaired Student's *t* test was used to analyse the significance of the difference between the two groups and ANOVA was used to analyse the significance of the difference between the groups (>2). **E** The ratio of M2 (F4/80+CD206+) subtype in the lysate, CFS, and untreated groups of CT26, MC38, and 4T-1 cells detected by flow cytometry. The data are averages from three samples per treatment group. An unpaired Student's *t* test was used to analyse the significance of the difference between the groups. **F** The phagocytic and killing functions of macrophages treated with different cancer cell lysates detected by CFSE/PI. Three effectors to target ratios were set for each cell line (RAW264.7: tumour cells=25:1, 50:1, and 100:1). The data are averages from three samples per treatment group. Statistical analysis was performed using ANOVA with multiple comparisons. ns, no significant differences, *, *p*<0.05, **, *p*<0.01, ***, *p*<0.001, ****, *p*<0.0001



of OH2 (Additional file 3: Fig. S1) or frozen cell lysate (Additional file 3: Fig. S2) could not activate macrophages directly within 24 h.

Subsequently, we used flow cytometry to detect the ratio of M1 (F4/80+CD86+) and M2 (F4/80+CD206+) macrophages after lysate treatment (Fig. 1C). The proportion of M1 macrophages after lysate and CFS treatment significantly increased ($p=0.0015$, $p<0.0001$, and

$p<0.0001$ for CT26, MC38 and 4T-1 lysate treatment, respectively, and $p=0.01$, $p=0.0073$, and $p=0.023$ for CT26, MC38, and 4T-1 CFS treatment, respectively) compared with the untreated group (Fig. 1D). There were also significant differences between the lysates and CFS treatment ($p=0.01$, $p=0.0018$, and $p<0.0001$ for CT26, MC38, and 4T-1 lysate treatment, respectively). Interestingly, there was no difference in the proportion

of M2 macrophages between the lysate and untreated groups, but the proportion of M2 macrophages in the CFS increased significantly compared with that in the other two groups (Fig. 1E, Additional file 3: Fig. S3). The ratio of M1 (F4/80+CD86+) and M2 (F4/80+CD206+) macrophages in RAW264.7 cells treated with lysate in the blocked SIRP α group and the nonblocked SIRP α group was not significantly different ($p=0.010$, Additional file 3: Fig. S4). The difference in RAW264.7 polarization induced by frozen cell lysate and CFS was not statistically significant (Additional file 3: Fig. S5). Similar results were also observed in mouse splenic primary macrophages. CFS did not significantly change the proportion of M1 or M2, while the proportion of both M1 and M2 in primary macrophages increased significantly after lysate treatment ($p<0.0001$). Although frozen cell lysate also increased the proportion of M1, it was more reflected in the proportion of M2 (Additional file 3: Fig. S6). These results indicated that the lysates effectively stimulated macrophages to polarize towards the M1 but not the M2 phenotype. To uncover the relationship between macrophage polarization and phagocytosis, a cell killing assay was performed. There were no significant differences between the CFS and untreated groups. Lysate-polarized M1 macrophages had a significant killing effect compared with the other two groups, and the effect was enhanced with an increase in the effector cell:target cell ratio (E:T) (Fig. 1F).

To explore the changes in macrophages with polarization, RNA sequencing was performed on different RAW264.7 treatment groups. Whether CT26 lysates were compared with supernatant or untreated RAW264.7 cells, GO analysis showed that the lysates activated the activity of antiviral signalling pathways in RAW264.7 cells, including response to virus, regulation of viral process, regulation of innate immune response, and response to interferon-beta (Fig. 2A and B). KEGG

analysis showed the same signalling changes as lysate treatment (Fig. 2C and D). Furthermore, GSEA showed that interferon-related pathways were upregulated and cell proliferation-related signalling pathways were downregulated after lysate treatment (Fig. 2E). Compared with the supernatant group, the expression of M1 markers (Il23a, Il6, Nfkb1, Cd80, Il27, Ccl5, Cd86, Il21r, Il33, Ccl6, Cxcl10, Il7, Cxcl11, Il18, Ccl7, Tlr4, and Ccl2) in the lysate treatment group was upregulated, and the expression of M2 markers (Stat3, Mr1, and Ncan) was downregulated (Fig. 2F and G). These results suggested that lysate treatment could effectively induce polarization of M1 macrophages, activate the function of M1 macrophages, and activate antiviral and antitumour immune responses.

OH2 treatment polarized macrophages to the M1 phenotype for tumour killing in vivo

We explored the correlation between OH2 treatment and macrophage function in vivo, as shown in Fig. 3A. Based on previous research [16], we showed that OH2 therapy promoted the infiltration of adaptive immune cells (T cells) and innate immune cells (macrophages, DCs and NK cells) (Fig. 3B).

Macrophages in CT26-bearing mice were cleared using clodronate liposomes (CLs) one day before treatment. First, we verified the clearance efficiency and found it reached more than 90% within 24 h after the injection and then recovered and was higher than the preinjection level 72 h later (Additional file 3: Fig. S7). These results suggest that the use of CL alone can effectively remove any existing macrophages without affecting the formation of new macrophages.

As shown in Fig. 3C, both OH2 therapy and CL combined with OH2 therapy showed strong tumour inhibition. Indeed, the combination therapy showed earlier tumour suppression and a more significant therapeutic effect ($p<0.0001$) (Fig. 3C). However, there was no

(See figure on next page.)

Fig. 3 OH2 treatment polarized macrophages to the M1 phenotype for tumour killing in vivo. **A** The treatment process and experiment timeline of the CL animal model. **B** The immune cell infiltration analysis results of the OH2 treatment group and control group by GSVA. **C** The tumour growth curve of the OH2 combined CL group (red), OH2 (OH2 with control liposomes) group (blue), and control group (black). The red box zoomed (right) in to show the OH2 combined CL group and OH2 group. Two-way analysis of variance (ANOVA) was performed on the experimental data. $n=10$ mice/group, ****, $P<0.0001$. **D** The survival curve of the OH2 combined CL group (red), OH2 group (blue), and control group (black). The Kaplan-Meier method and log-rank test were used for the survival curve data. ns, no significant differences. **E** Representative M-IHC results of the OH2 group (left) and OH2 combined CL group (right). F4/80, green, CD86, purple, and CD206, yellow. Scale bar, 100 μ m. **F** M-IHC quantification results for M1 subtype. $n=3$ samples/group. The Student's t test was used to analyse the significance of the difference between the two groups. ****, $p<0.0001$. **G** M-IHC quantification results for M2 subtype. $n=3$ samples/group. The Student's t test was used to analyse the significance of the difference between the two groups. **, $p<0.01$. **H** Representative IHC staining for CD86 (left), CD206 (middle), and F4/80 (right) in the OH2 (top) and OH2 combined CL group (bottom). Original magnification, $\times 200$. $n=5$ samples/group. (Percentage represented the proportion of M1/M2 macrophages in the total number of cells). **I** Quantitative results of CD86 staining in the OH2 combined CL and OH2 group. **J** Quantitative results of CD206 staining in the OH2 combined CL and OH2 group. **K** Quantitative results of F4/80 staining in the OH2 combined CL and OH2 group. $n=3$ samples/group. The Student's t test was used to analyse the significance of the difference between the two groups. ns, no significant differences, *, $p<0.05$, **, $p<0.01$, ***, $p<0.001$, ****, $p<0.0001$

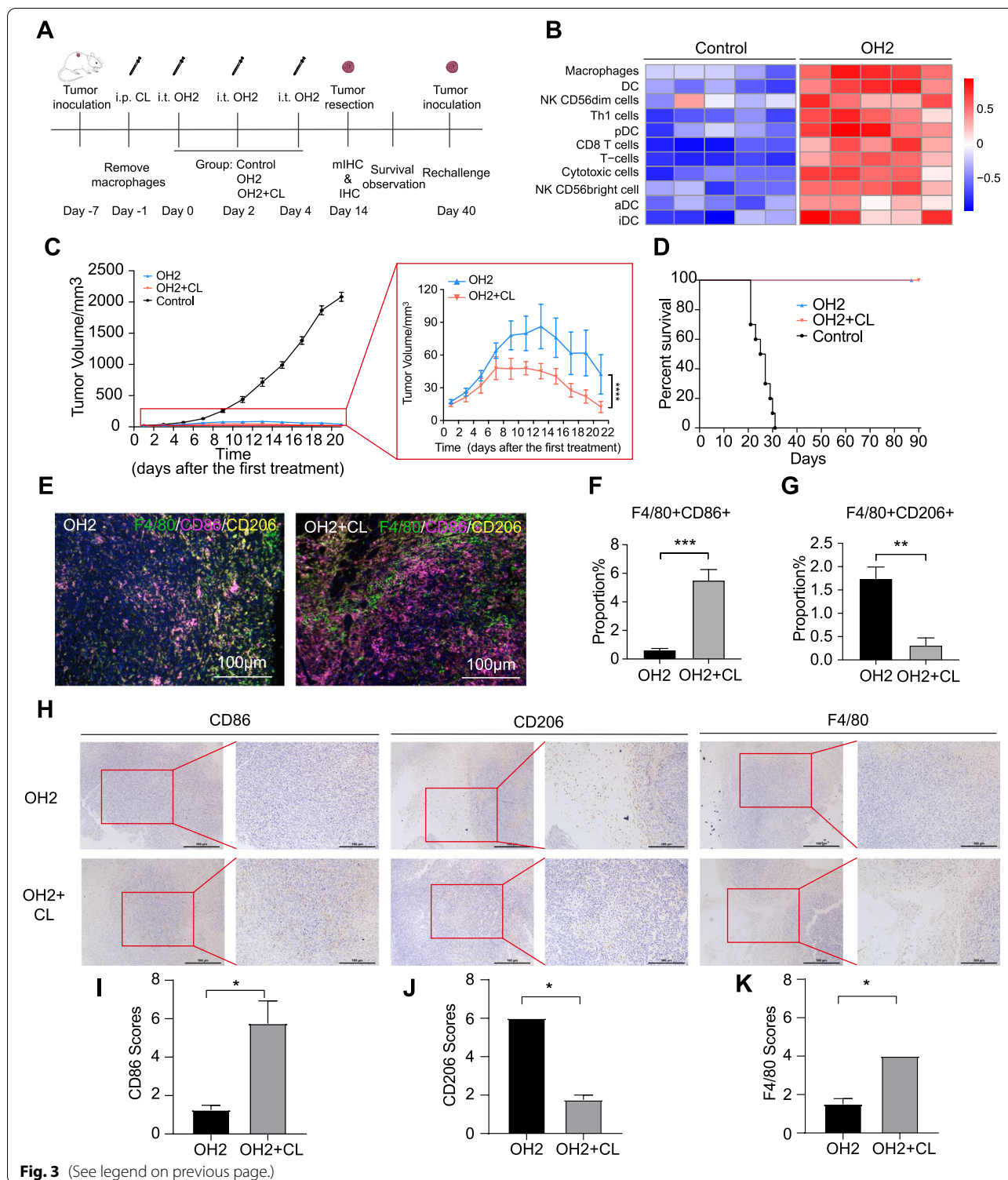


Fig. 3 (See legend on previous page.)

difference in survival between the two groups, and all of the tumours in the combined and OH2 groups ultimately regressed (Fig. 3D). The rechallenge experiment showed that the tumour formation rate of the combined

group was significantly lower than that of the OV group ($p=0.029$), although the tumours eventually returned (Additional file 3: Fig. S8). This implies that macrophages might play a role in the treatment effect of OH2.

Quantitative analysis by multicolour immunohistochemistry (M-IHC) showed that the combined use of CL and OH2 promoted an increase in M1 macrophages ($p=0.0004$) in the tumour immune microenvironment, accompanied by a decline in M2 macrophages ($p=0.0011$) compared with OH2 alone (Fig. 3E–G, Additional file 3: Fig. S9). The immunohistochemistry results showed that the M1 macrophage marker was highly expressed in tumour tissues, and the M2 macrophage marker was only expressed at low levels in the combination therapy group (Fig. 3H–K). These results suggested that OH2 therapy can induce polarization of M1 macrophages and participate in the antitumour immune response in vivo.

Combined anti-SIRP α therapy with OH2 enhances anticancer immune responses in a CT26 cancer model

To further explore the feasibility of OH2 combined with macrophage therapy, an anti-SIRP α antibody that blocks the CD47-SIRP α axis in macrophages was used. First, we detected the expression of CD47 and SIRP α in cell lines. As shown in Fig. 4A, CD47 was widely expressed in most cell lines, while SIRP α expression was cell-line specific. The expression level of SIRP α on macrophages in the spleens of mice was shown in Additional file 3: Fig. S10. These results suggested that we could remove the blocking effect of CD47 on macrophage phagocytosis with an anti-SIRP α antibody.

An in vivo test was performed. When the CT26 tumour volume was small at the start of treatment ($45.315 \pm 4.403 \text{ mm}^3$), the tumour volume and survival were not significantly different between the combined treatment group and the OH2 treatment group ($p=0.4712$) (Additional file 3: Fig. S11). Whether as a single or combined treatment, OH2 could exert excellent antitumour efficacy, and the tumour would eventually regress completely. Then, we adjusted the in vivo experiment (Fig. 4B). We started treatment on day 14 when the tumour was larger ($281.596 \pm 31.469 \text{ mm}^3$), and a difference in efficacy

between the OV treatment group and the combined treatment group began to appear (Fig. 4C). Compared with the other groups, the tumours in the combined treatment group regressed faster. In addition, mice in the combination group had a higher survival rate ($P=0.041$) than mice in the OH2 and OH2+isotype groups (Fig. 4D). The number of mice that achieved tumour regression was also the largest. Compared with the control group, both groups using OH2 were able to effectively inhibit tumour growth and prolong the survival of the mice (Fig. 4E, F). However, the anti-SIRP α antibody alone neither inhibited tumour growth ($P>0.05$, Fig. 4E) nor prolonged the survival time of tumour-bearing mice ($P>0.05$, Fig. 4F).

We also verified immune exclusion in 4T-1 mouse models (Fig. 4G). As shown in Fig. 4H, the combination group showed a potent antitumour effect that was significantly different from the OH2 group ($p=0.0041$) and the control group ($p=0.003$). In addition, mice in the combination group had a better survival rate than mice in the OH2 ($p=0.03$) and control groups ($p=0.0014$) (Fig. 4I). These results showed that the anti-SIRP α antibodies enhanced the efficacy of OH2 therapy.

Subsequently, we performed a pathological analysis of the tumour tissue from the mice. The pathological results showed that in the tumour microenvironment of mice that did not receive treatment, the proportion of M2 macrophages was much higher than that of M1 macrophages (Fig. 5A, Additional file 3: Fig. S12). Treatment with OH2 reduced the infiltration of M2 macrophages ($p<0.001$) and increased the infiltration of NK cells ($p<0.05$) into the tumour microenvironment to a certain extent (Fig. 5B and C). The combined use of anti-SIRP α antibody and OH2 resulted in increased infiltration of CD8 T cells ($p<0.01$) and M1 macrophages ($p<0.001$) into the tumour microenvironment (Fig. 5D and E). The immunohistochemistry results showed that the immune cells of the combined treatment group were concentrated in the central part of the tumour (Fig. 5F, G and

(See figure on next page.)

Fig. 4 The combination of OH2 and anti-SIRP α therapy enhances anticancer immune responses in vivo. **A** The expression levels of CD47 and SIRP α in CT26, MC38, and 4T-1 cell lines were detected by flow cytometry. **B** The treatment process and the experimental timeline for adjusted combined treatment. **C** The tumour growth curve of different treatment groups of tumour-bearing mice with larger tumour volumes at the initial treatment. The red box zoomed in to show the OH2 combined anti-SIRP α antibody group, OH2 combined isotype, and OH2 group. Two-way analysis of variance (ANOVA) was performed on the experimental data. $n=10$ mice/group. *, $p=0.019$. **D** The survival curve of different treatment groups of tumour-bearing mice with larger tumour volumes at the initial treatment. The Kaplan-Meier method and log-rank test were used for the survival curve data. *, $p=0.041$. **E** The tumour growth curve of the OH2 combined anti-SIRP α antibody group, anti-SIRP α antibody group, OH2 group, and control group. Two-way analysis of variance (ANOVA) was performed on the experimental data. $n=6$ mice/group. *, **. **F** The survival curve of the OH2 combined anti-SIRP α antibody group, anti-SIRP α antibody group, OH2 group, and control group. The Kaplan-Meier method and log-rank test were used for the survival curve data. *, $p=0.0183$. **G** The treatment process and experimental timeline for the combined treatment. **H** The tumour growth curve of the OH2 combined anti-SIRP α antibody group, OH2 combined isotype, and control group. Two-way analysis of variance (ANOVA) was performed on the experimental data. $n=7$ mice/group. *, $p=0.029$; **, $P=0.0041$; ***, $p=0.0003$. **I** The survival curve of the OH2 combined anti-SIRP α antibody group, OH2 combined isotype, and control group. The Kaplan-Meier method and log-rank test were used for the survival curve data. *, $p=0.03$ and $p=0.018$; **, $P=0.0014$

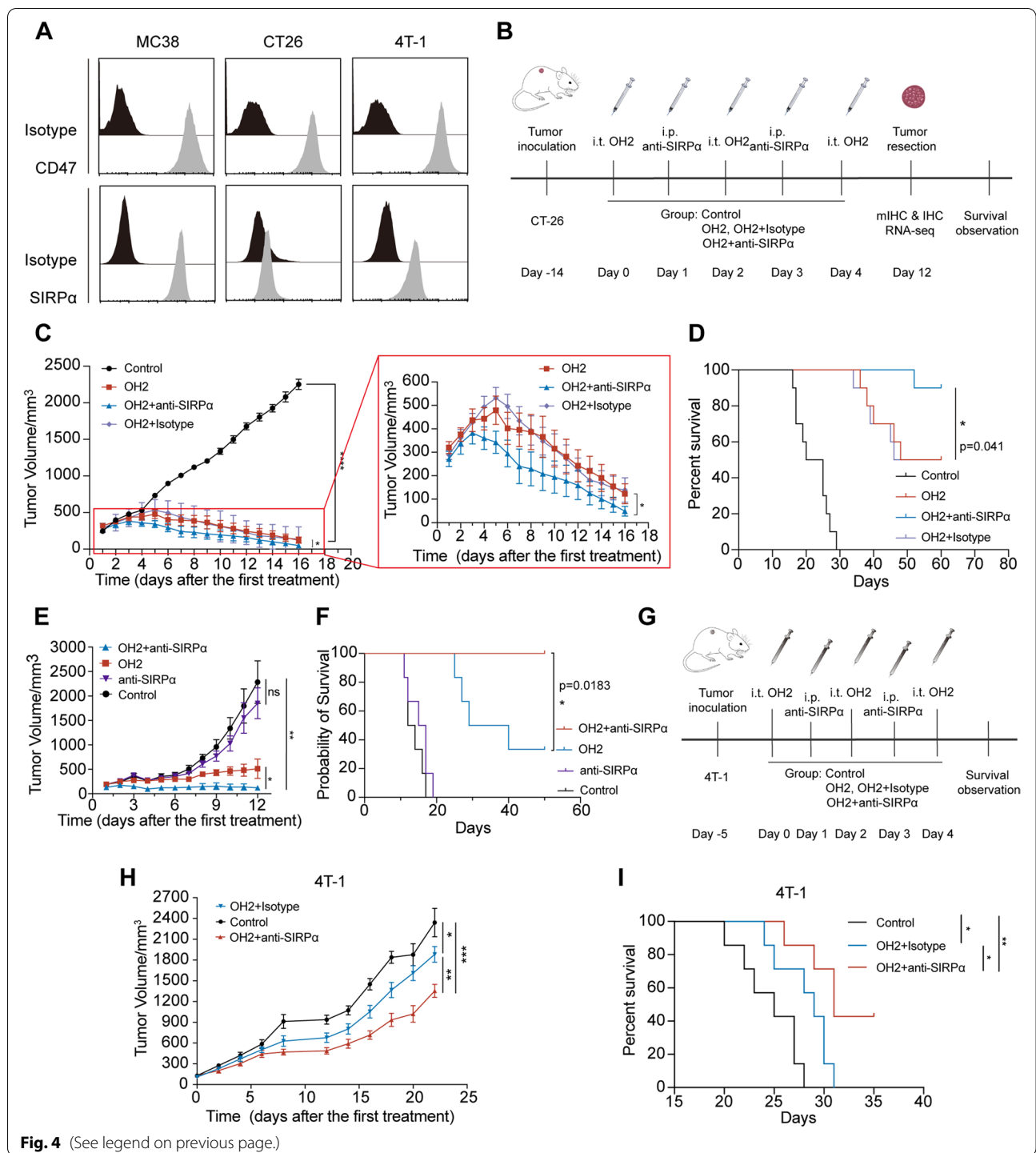


Fig. 4 (See legend on previous page.)

Additional file 3: Fig. S13). This implied that the ability of these tumour-inhibiting immune cells to migrate to the centre of the tumour was enhanced. These results suggested that combination therapy can stimulate a stronger antitumour immune response than treatment alone.

Combination therapy reshapes the TME and activates a more comprehensive antitumour immune response. We used RNA sequencing and single-RNA sequencing to characterize the TME in more detail. OH2 treatment alone can promote the infiltration of adaptive

immune cells (T cells and Th1 cells) and innate immune cells (macrophages and DCs) into the tumour immune microenvironment (Fig. 6A). In the combination therapy group, the scores of macrophages were much higher. Although there was no significant difference, DCs, CD8+, and cytotoxicity were improved by the combination compared to OH2 treatment alone (Fig. 6B). When anti-SIRP α and OH2 were combined, they were more conducive to the infiltration of immune cells into tumour tissues, especially macrophages, DCs, T cells, and NK cells. Immune cells were globally activated, thereby creating an antitumour tumour microenvironment (Fig. 6C). As a result of immune cell infiltration, the antigen presentation signal in the tumours of the combined treatment group was enhanced, and the killing function of the immune cells was strengthened (Fig. 6D, and Additional file 3: Fig. S14). However, the proliferation ability of the tumour cells decreased, and apoptosis increased (Fig. 6C, Additional file 3: Fig. S15). The GO analysis showed that leukocyte migration and chemotaxis were enhanced in the combined treatment group, consistent with the IHC results (Fig. 6E and F). The enhanced migration ability and functional activation of immune cells in tumour tissues, as well as the full activation of M1-related cytokines, T cell-related cytokines, and NK-related cytokines, promoted the elimination of tumour cells (Fig. 6G–I). These results suggested that combination therapy can more profoundly reshape the TME and activate stronger innate and adaptive immune responses.

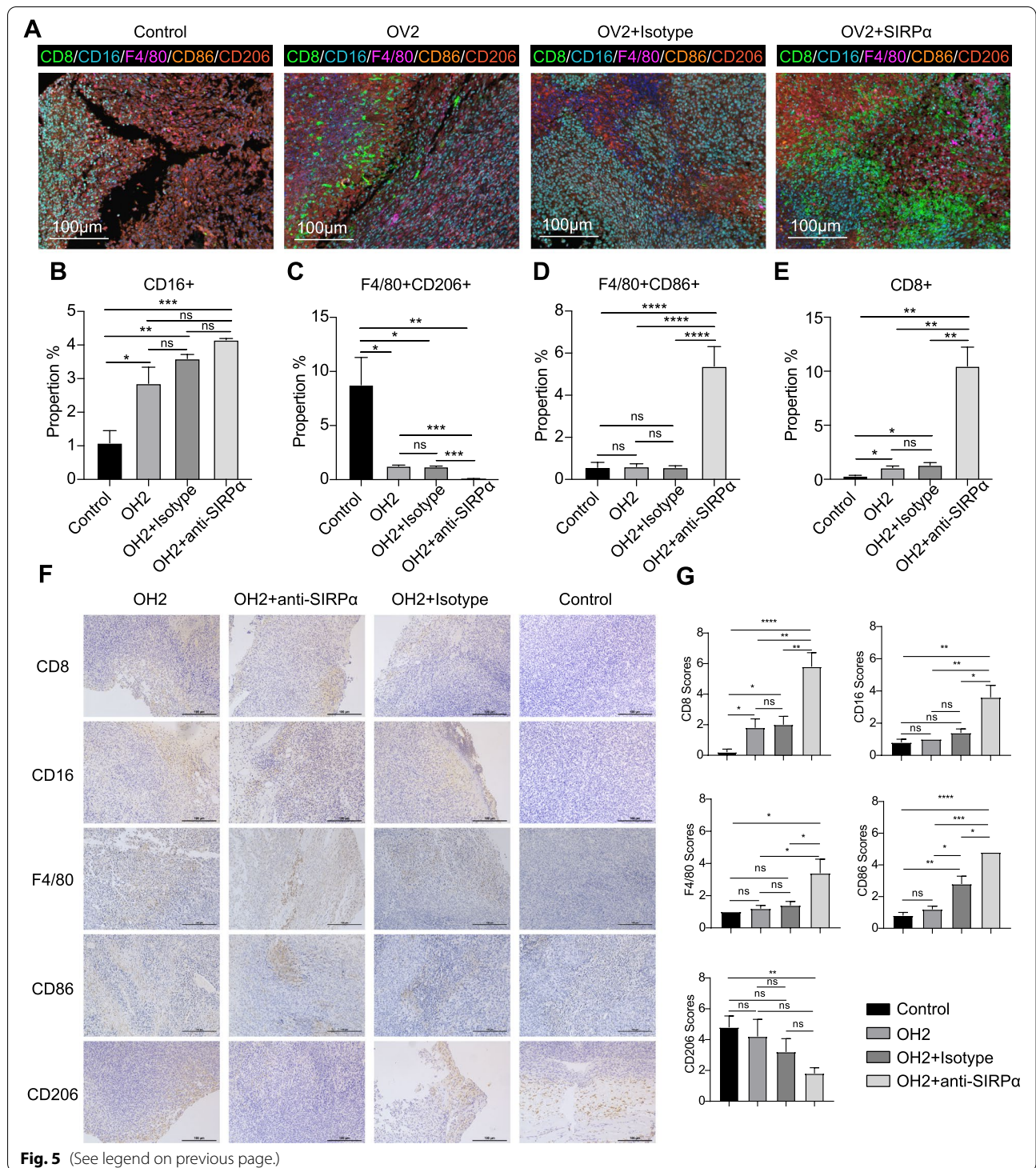
The single-cell data showed that immune cells in the tumour microenvironment could be divided into T cells, B cells, NK cells, myeloid cells, mast cells, and DC cells (Fig. 7A, and Additional file 3: Fig. S16). The proportion of each immune cell subset is shown in Fig. 7B. Compared with the control group, the T cells, NK cells and DC cells in the OH2 group and the OH2 combined anti-SIRP α antibody group increased, while the myeloid cells decreased. Compared with the group treated with OH2 alone, NK cells and DC cells were significantly

increased in the combination treatment group, and myeloid cells were significantly decreased (Fig. 7B). Analysis of the different types of macrophages showed that (Fig. 7C) M1 macrophages were increased in both groups treated with OH2, but the increase in M1 macrophages was more significant in the combined treatment group (Fig. 7D). The genes differentially expressed between the OH2 combined anti-SIRP α antibody group and the two other groups were identified. Virus nucleic acid fragments, unpackaged intact capsid proteins, or cellular contents might be involved in the treatment as PAMPs/DAMPs. The results of single-cell sequencing data showed that Tlr2 and Tlr13 are upregulated (Fig. 7E). Tlr2 and Tlr13 recognize virus components and activate Toll-like receptor (TLR)-dependent signalling pathways [22, 23], and the function of immune cells was strongly activated (Fig. 7F).

To verify the tumour-specific cytotoxic T lymphocyte (CTL) response of treatment, the spleen lymphocytes isolated from different treatment groups (control, anti-SIRP α , OH2, and OH2+ anti-SIRP α) were co-cultured with CT26 cells in vitro at target cell/effector cell (T:E) ratios of 1:100, 1:50, and 1:25. Lymphocytes from both the OH2 group and the OH2+ anti-SIRP α group showed a highly specific CTL response against CT26 cells ($p < 0.001$). The CTL response of OH2 combined with anti-SIRP α antibody was more intense than that of OH2 alone ($p < 0.05$). However, no CTL response was detected with anti-SIRP α antibody alone (Additional file 3: Fig. S17A). ELISA was used to detect the supernatant of co-cultured cells, and we found that the expression of TNF- α , Granzyme B and IFN- γ could be significantly induced in the OH2 group and the OH2+anti-SIRP α group ($p < 0.0001$, Additional file 3: Fig. S17B). Overall, T cell effector cytokines were slightly higher in the OH2+anti-SIRP α group than in the OH2 group, although there was no statistical difference. Also, T cell effector cytokines were not detected with anti-SIRP α antibody alone. These results suggested that combination therapy can also improve the tumour-specific CTLs.

(See figure on next page.)

Fig. 5 M-IHC and IHC staining of the anti-SIRP α antibody treatment model. **A** Representative M-IHC results of the OH2 combined anti-SIRP α antibody group, OH2 combined isotype, OH2 group, and control group with larger tumour volume at the initial treatment. CD8, green, CD16, sky blue, F4/80, purple, CD86, orange, and CD206, red. Scale bar, 100 μ m. **B** Quantitative results of NK cell (CD16) staining in the OH2 combined anti-SIRP α antibody group, OH2 combined isotype, OH2 group, and control group. $n=3$ samples/group. **C** Quantitative result of M2 macrophage (F4/80+CD206+) staining in the OH2 combined anti-SIRP α antibody group, OH2 combined isotype, OH2 group, and control group. $n=3$ samples/group. **D** Quantitative results of M1 macrophage (F4/80+CD86+) staining in the OH2 combined anti-SIRP α antibody group, OH2 combined isotype, OH2 group, and control group. $n=3$ samples/group. **E** Quantitative results of CD8 T cell staining in the OH2 combined anti-SIRP α antibody group, OH2 combined isotype, OH2 group, and control group. $n=3$ samples/group. **F** Representative IHC staining for CD8, CD16, F4/80, CD86, and CD206 of the OH2 combined anti-SIRP α antibody group, OH2 combined isotype group, OH2 group, and control group with larger tumour volumes at the initial treatment. Original magnification, $\times 200$. $n=5$ samples/group. **G** Quantitative results of CD8, CD16, F4/80, CD86 and CD206 staining in the OH2 combined anti-SIRP α antibody group, OH2 combined isotype, OH2 group and control group. $n=5$ samples/group. Statistical analysis was performed using ANOVA with multiple comparisons. ns, no significant differences, *, $p < 0.05$, **, $p < 0.01$, ***, $p < 0.001$, ****, $p < 0.0001$ (proportion represented the percentage of the cell to the total number of cells)



Discussion

We report the efficacy and molecular and immunological effects of combination therapy with oncolytic herpes simplex virus and anti-SIRPα in a mouse model in vitro and in vivo (Fig. 8). We demonstrated that

tumour cell lysate-induced OH2 can effectively activate and induce the differentiation of mouse RAW264.7 macrophages towards the M1 phenotype, enhancing their phagocytosis and killing effects on tumour cells in vitro. We observed that the combination of OH2 and

anti-SIRP α , which blocks the CD47-SIRP α axis, can effectively enhance the therapeutic effect by enhancing the innate immune effect of macrophages. The combination of OH2 and anti-SIRP α also showed stronger regulation of the tumour immune microenvironment.

In recent years, OV s have been considered a promising new strategy for cancer treatment. Compared with surgical therapy, chemoradiotherapy and targeted therapy, OV s have shown high killing ability, precise targeting ability, and few side effects or drug resistance [9, 24, 25]. OV s can be genetically modified to enhance their tumour targeting ability, improve their safety, and increase their antitumour efficacy [26, 27]. More than 40 OV types are currently being evaluated in clinical trials for the treatment of various tumours, most of which are in phase I studies [24], but only T-VEC has successfully entered phase III clinical trials and received marketing approval [28].

The OH2 used in the current study showed good intratumoural injection tolerance and persistent antitumour activity in patients with metastatic oesophageal and rectal cancer in a recent study [29]. Although a large number of clinical trials have shown positive results with OV s , their efficacy as monotherapy agents is limited [6, 30, 31]. Therefore, combination therapy is one of the strategies used to enhance the therapeutic effect of OV s [32, 33].

The mechanism by which OV kills tumours includes infection and replication in tumour cells, leading to the lysis or apoptosis of the tumour cells, and a more important mechanism is the killed tumour cells release tumour-related antigens to achieve an enhanced tumour-specific immune response [34]. Since OV therapy can induce an adaptive antitumour immune response, a combination of immune checkpoint inhibitors (ICIs) and OV s could have potential clinical value. Some studies have shown that OV combined with CTLA-4 inhibitors or PD-1 inhibitors improves the antitumour response and significantly improves patient survival, both in preclinical studies and clinical trials [2, 35–38]. Currently, there are 19 ongoing clinical trials of ICI and OV combination therapy,

showing that combination therapy has become one of the hot spots of OV clinical treatment options [39].

However, the existing combination therapy focuses more on the adaptive immune response and less on innate immunity. When OV s lyse tumour cells, they release many cytokines, pathogen-associated molecular patterns (PAMPs) and damage-associated molecular patterns (DAMPs), which activate innate immune responses. Our data showed that the lysate of OH2 after infection with tumour cells could effectively stimulate mouse macrophage line RAW264.7 activation and M1-like polarization in vitro. Although RNA sequencing results showed that RAW264.7 cells had a strong antiviral immune response, M1-like polarized RAW264.7 cells also showed significant tumour-specific killing ability in subsequent experiments. Saha et al. [40] showed that ICI combined with OV modestly extended the survival of a mouse glioma model, which was associated with macrophage influx and M1-like polarization. These results suggest that OV combined with innate immune cells, such as macrophages and dendritic cells, also has potential application value.

Recent studies have shown that the CD47-SIRP α axis is a phagocytic checkpoint regulating macrophages and other innate immune cells, and a series of molecules that block the CD47-SIRP α axis are in clinical development for tumour therapy [13, 41]. Some research groups have engineered oHSV1 expressing a full-length CD47 antibody, which has achieved good therapeutic efficacy in mouse models of metastatic ovarian cancer and glioblastoma [42, 43]. Yao et al. [44] reported the antitumour effect of a novel oncolytic adenovirus containing the SIRP α -IgG1 Fc fusion gene in CD47-positive cancer. Since CD47 is commonly expressed at high levels in normal tissues, specific targeting of tumour cells via CD47 is questionable [45]. SIRP α is highly expressed in bone marrow cells such as macrophages and DCs but is expressed at low levels in other immune cells. Therefore, SIRP α may be a more ideal target for the CD47-SIRP α axis [45, 46]. In this study, we demonstrated that oncolytic

(See figure on next page.)

Fig. 6 The tumour immune microenvironment revealed by RNA sequencing results of tumour tissues in different treatment groups. **A** The immune cell infiltration analysis results of tumour tissues from the OH2 combined anti-SIRP α antibody group, OH2 group, and control group by GSVA. **B** The scoring results of immune cells (macrophages, DCs, Th1 cells, Th2 cells, T cells, CD8 T cells, NK CD56bright cells, and cytotoxic cells) of tumour tissues from the OH2 combined anti-SIRP α antibody group, OH2 group, and control group by GSVA. **C** The immune-related signalling pathways of tumour tissues from the OH2 combined anti-SIRP α antibody group, OH2 group, and control group by GSVA. **D** The scoring results of immune-related signalling pathways (interferon, NK cell activity, cytotoxicity, T cell priming, and activation, immune cell localization to tumours, cytokine, and chemokine signalling) of tumour tissues from the OH2 combined anti-SIRP α antibody group, OH2 group, and control group by GSVA. **E** GO analysis of differentially expressed genes in the control group and the OH2 combined anti-SIRP α antibody group. **F** GO analysis of differentially expressed genes in the OH2 group and the OH2 combined anti-SIRP α antibody group. **G** The expression level of M1-related cytokines in the OH2 group, OH2 combined with anti-SIRP α antibody group and control group. **H** The expression levels of T cell-related cytokines in the OH2 group, and OH2 combined with the anti-SIRP α antibody group and the control group. **I** The expression level of NK-related cytokines in the OH2 group, OH2 combined with anti-SIRP α antibody group and control group. An unpaired Student's *t* test was used to analyse the significance of the difference between the two groups. ns, no significant differences, *, $p < 0.05$, **, $p < 0.01$, ***, $p < 0.001$, ****, $p < 0.0001$. The colour represents the value of the expression level of the gene in RNA sequencing. OH2 + SIRP α represents the OH2 combined with the anti-SIRP α antibody group

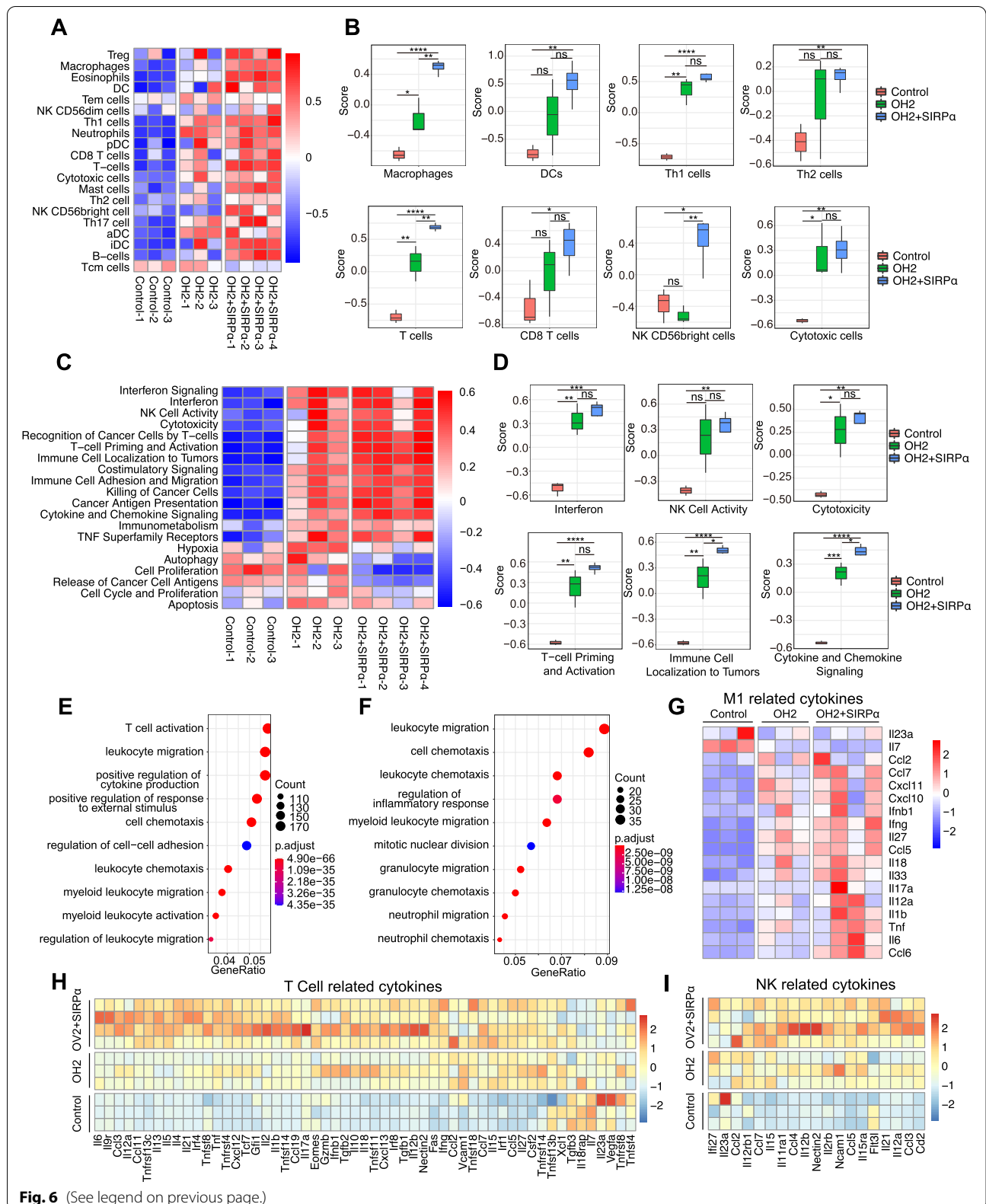
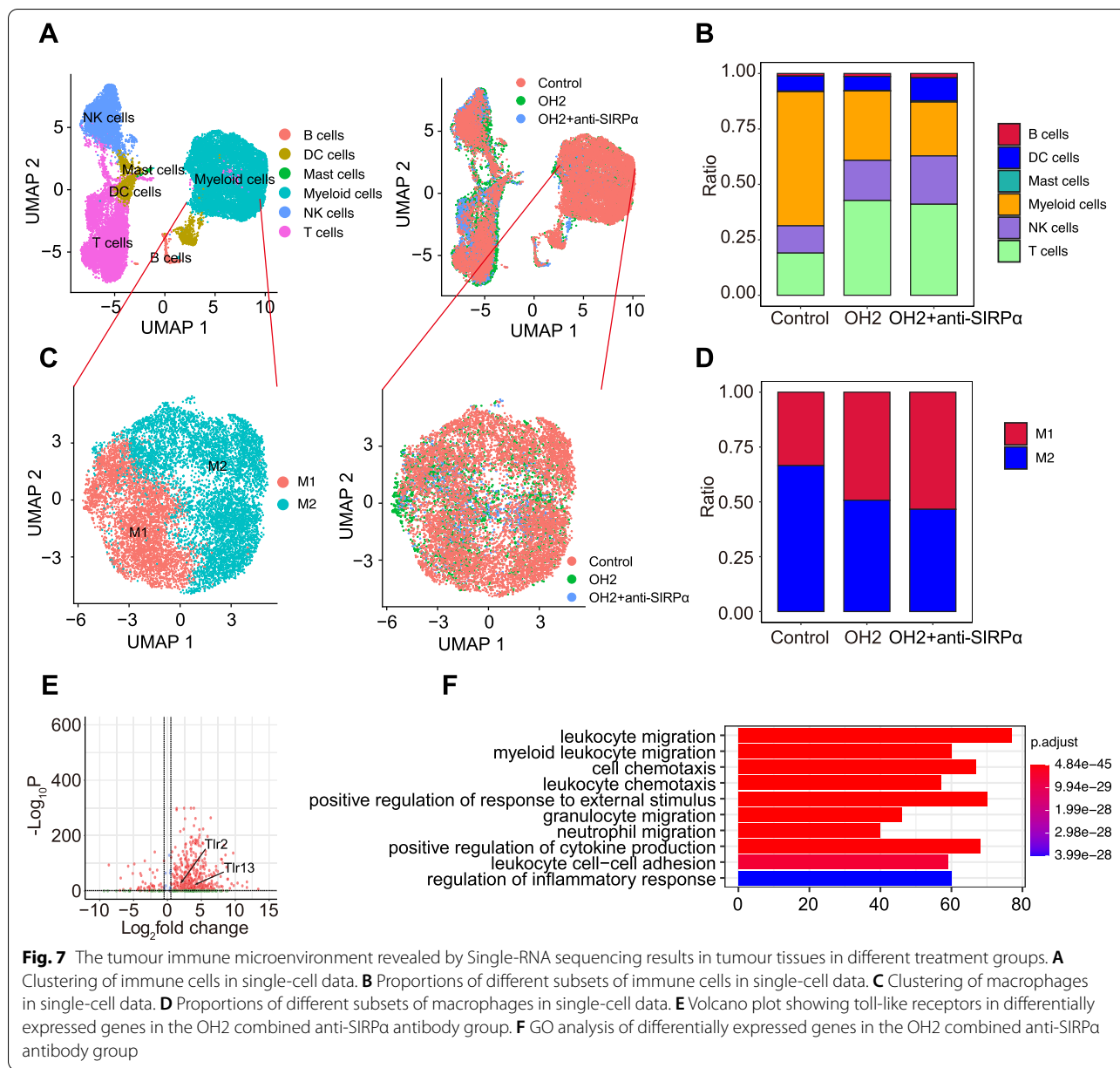


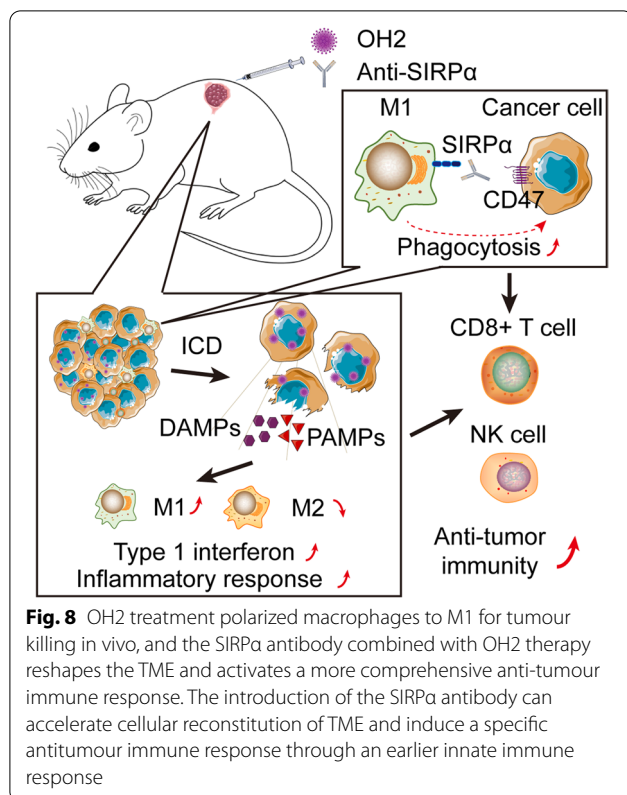
Fig. 6 (See legend on previous page.)



virus therapy could effectively recruit and activate macrophages in vivo and induce M1-like polarization, demonstrating the feasibility of blocking OV in combination with blocking the CD47-SIRPα axis. The combination of OH2 and anti-SIRPα antibodies had a significant effect on the treatment of the mouse colorectal cancer CT-26 model. Interestingly, we found that the combination therapy was more effective in mice with larger initial tumour volumes. This may be due to the number of infiltrated monocytes in the tumour microenvironment with increasing tumour size, and oncolytic virus treatment switched the tumour microenvironment from “cold” to “hot”, thus inducing the generation of more abundant

M1-like macrophages. These results also suggest that the therapeutic effect can be further improved by optimizing different dosing times of combination therapy.

With better understanding of the tumour immune microenvironment, immunotherapy based on macrophages is becoming a reality [47]. Macrophages are important regulators of many aspects of the TME and can activate tumour-specific immune responses directly or through nonspecific effects on T and B-cell functions [12, 48, 49]. We also observed that either OV therapy alone or in combination with SIRPα antibody recruited large numbers of NK cells and monocytes to trigger innate immune responses, which is consistent with the findings of



Ramelyte et al. [50]. Macrophages play an important role in limiting HSV infection [51, 52], and the single-cell sequencing results showed activation of TLR signalling pathways involved in the combination therapy group. We observed that the combination therapy did not produce a significant antiviral response compared with treatment alone, however, macrophages are more likely to activate the overall immune state. The results suggest that the combination therapy induces a more specific killing of tumour cells. The characteristics of combination therapy at the cellular and molecular levels are based on the rapid reconstruction of the immune environment within the TME and the comprehensive and continuous activation of innate and adaptive immunity. The effectiveness of combination therapy is due to multiple immune synergies, not just one type of immune cell. Macrophages may play a role in early antigen presentation and an expanded immune response.

Conclusions

In conclusion, our data support the feasibility of oncolytic virus therapy in combination with an anti-SIRPα antibody. The introduction of the anti-SIRPα antibody can accelerate cellular reconstitution of the TME and induce a specific antitumour immune response through an earlier innate immune response. Our study suggests a new strategy for oncolytic virus therapy.

Abbreviations

SIRPα: Signal regulatory protein-alpha; OH2: Oncolytic herpes simplex virus 2; OV: Oncolytic virus; RNA-seq: RNA sequencing; TME: Tumour microenvironment environment; ICB: Immune checkpoint blockade; ICD: Immunogenic cell death; DAMPs: Damage-associated molecular patterns; PAMPs: Pathogen-associated molecular patterns; CFS: Cell-free supernatant; CCK8: Cell Counting Kit-8; GO: Gene ontology; KEGG: Kyoto Encyclopedia of Genes and Genomes; GSEA: Gene set enrichment analysis; CL: Clodronate liposomes; M-IHC: Multicolour immunohistochemical; IHC: Immunohistochemical; SPF: Specific pathogen free; TLR: Toll-like receptor; CTL: Cytotoxic T lymphocyte.

Supplementary Information

The online version contains supplementary material available at <https://doi.org/10.1186/s12916-022-02574-z>.

Additional file 1: Table S1. Gene list for heatmap.

Additional file 2: Table S2. GSEA gene list.

Additional file 3: Figure S1. Cell proliferation assay results. Cell proliferation assay results of Raw264.7 cell lines treated with OH2 MOI=1 (red), OH2 MOI=0.5 (blue) and untreated (black) group by CCK8 assay in 72 hours. **Figure S2.** OH2 lysates induce RAW264.7 polarization and phagocytosis in vitro. A. Demonstration of the analysis of the phagocytosis by flow cytometry. B. Cell proliferation assay results of CT26, MC38 and 4T-1 cell lines treated with lysate (red), CFS (blue), Cell frozen lysate (purple) and untreated (black) group by CCK8 assay in 24 hours. **, $p < 0.01$. **Figure S3.** The ratio of M1 (F4/80+CD86+) and M2 (F4/80+CD206+) macrophages in RAW264.7 without any treatment by flow cytometry. **Figure S4.** The ratio of M1 (F4/80+CD86+) and M2 (F4/80+CD206+) macrophages in RAW264.7 treated with lysate in the blocked SIRPα group and the non-blocked SIRPα group. A. Demonstration of the analysis of the polarization of macrophages by flow cytometry. B. Display of isotype control results for different antibodies. C. The ratio of M1 (F4/80+CD86+) and M2 (F4/80+CD206+) macrophages in the blocked SIRPα group and the non-blocked SIRPα group. D. The ratio of M1 (F4/80+CD86+) and M2 (F4/80+CD206+) macrophages in the blocked SIRPα group and the non-blocked SIRPα group. An unpaired Student's t test was used to analyze the significance of the difference between two groups. **Figure S5.** Cell frozen lysate and CFS induce RAW264.7 polarization in vitro. A. Flow cytometric analysis results of one representative sample from each cell line. B. The ratio of M1 (F4/80+CD86+) subtype in the Cell frozen lysate and CFS groups of CT26, MC38 and 4T-1 cells detected by flow cytometry. An unpaired Student's t test was used to analyze the significance of the difference between two groups. **Figure S6.** OH2 lysates induce primary macrophages polarization in vitro. A. Demonstration of the analysis of the polarization of macrophages by flow cytometry. B. The percentage of M1 (F4/80+CD86+) subtype and M2 (F4/80+CD206+) subtype in the lysate, CFS, untreated and cell frozen lysate groups detected by flow cytometry. The data are averages from three samples per treatment group. Statistical analysis was performed using ANOVA with multiple comparisons. ns, no significant differences, *, $p < 0.05$, **, $p < 0.01$, ***, $p < 0.001$, ****, $p < 0.0001$. **Figure S7.** The clear efficiency of CL detected by flow cytometry. Statistical analysis was performed using ANOVA with multiple comparisons. ***, $p = 0.0003$; ****, $p < 0.0001$. **Figure S8.** Tumor-rechallenge with CT26 of the OH2 or OH2+ CL cured animals. A. The tumor growth curve of CT26 cells rechallenge after the tumors of the CL model had completely regressed. B. The tumorigenic rate of tumor-rechallenge mice in OH2 combined control liposomes group and OH2 combined CL group. Statistical differences were calculated using the Chi-square test. $p = 0.0291$. **Figure S9.** M-IHC staining of OH2 (left) and OH2 combined CL group (right) including each single staining marker. **Figure S10.** Expression level of SIRPα on macrophages in spleen from mice detected by flow cytometry. A. Demonstration of the expression level of SIRPα on macrophages in spleen from mice detected by flow cytometry. B. Histogram showing Expression level of SIRPα on macrophages in spleen from mice ($n = 3$). **Figure S11.** Combined anti-SIRPα therapy with OH2 enhances anticancer immune responses in a CT26 cancer model. A. The treatment process and experimental timeline for the combined treatment. B. The tumor growth curve of different treatment groups of tumor-bearing mice with smaller

tumor volumes at the initial treatment. The red box zoomed in to show the OH2 combined anti-SIRPa antibody group, OH2 combined isotype and OH2 group. Two-way analysis of variance (ANOVA) was performed on the experimental data. $n=10$ mice/group. ns, no significant differences. C. The survival curve of different treatment groups of tumor-bearing mice with smaller tumor volumes at the initial treatment. The Kaplan-Meier method and log-rank test were used for the survival curve data. ns, no significant differences. **Figure S12.** M-IHC staining results of anti-SIRPa model. M-IHC staining of control group (top left), OH2 group (top right), OH2 combined isotype group (bottom left) and OH2 combined anti-SIRPa antibody group (bottom right) including each single staining marker. **Figure S13.** IHC staining and quantitative results of the anti-SIRPa antibody treatment model. A. Representative IHC staining for CD8, F4/80, CD86 and CD206 of the OH2 combined anti-SIRPa antibody group, control group and anti-SIRPa antibody group with larger tumor volumes at the initial treatment. B. Quantitative results of CD8, F4/80, CD86 and CD206 staining in the the OH2 combined anti-SIRPa antibody group, control group and anti-SIRPa antibody group. Original magnification, $\times 200$. $n=5$ samples/group. Statistical analysis was performed using ANOVA with multiple comparisons. ns, no significant differences, *, $p<0.05$, **, $p<0.01$, ***, $p<0.001$, ****, $p<0.0001$. **Figure S14.** KEGG results of tumor tissues from anti-SIRPa model. A. KEGG results of differentially expressed genes between OH2 combined anti-SIRPa antibody group and control group. B. KEGG results of differentially expressed genes between OH2 combined anti-SIRPa antibody group and OH2 combined isotype antibody group. **Figure S15.** GSEA results of tumor tissues from anti-SIRPa model. A. GSEA results of differentially expressed genes between OH2 combined anti-SIRPa antibody group and control group. B. GSEA results of differentially expressed genes between OH2 combined anti-SIRPa antibody group and oHSV-2 combined isotype antibody group. **Figure S16.** scRNA-seq data analysis. A. UMAP plots represent the clusters (left) and groups (right) of tumor cells. B. A heatmap showing the scaled average expression of each cell subcluster. C. UMAP plots showing the expression values of canonical marker genes of each subcluster. D. A heatmap showing the scaled average expression of each immune cell subcluster. C. UMAP plots showing the expression values of canonical marker genes of each immune subcluster. **Figure S17.** CTL Assay. A. The killing functions of lymphocyte co-cultured with different cancer cell lysates detected by CFSE/PI. Three effectors to target ratios were set for each cell line (Lymphocyte: tumor cells = 25:1, 50:1, and 100:1). The data are averages from three samples per treatment group. Statistical analysis was performed using ANOVA with multiple comparisons. ns, no significant differences, *, $p<0.05$, **, $p<0.01$, ***, $p<0.001$, ****, $p<0.0001$. B. Supernatant from the CTL assay was tested for TNF- α , Granzyme B and IFN- γ by ELISA. Statistical analysis was performed using ANOVA with multiple comparisons. ns, no significant differences, ****, $p<0.0001$.

Additional file 4. Supplementary methods.

Authors' contributions

WZ, KTZ, and DFK designed the experiments. DFK conducted the experiments. DFK, WZ, and QYW performed data processing and statistical analysis. DFK, WZ, KTZ, and BLL wrote, reviewed, and/or revised of the manuscript. ZRY, GLL, ZRG, SW, QZ, ZLZ, and SJC provided administrative, technical, or material support (i.e. preparing surgical instrument for animal experiments, reporting or organizing data, and constructing databases). WZ and KTZ supervised the study. All authors read and approved the final manuscript.

Funding

This study was supported by the National Science Foundation of China (No. 82001758) and The Key Research and Development Program of Hubei province (2020BCA062).

Availability of data and materials

The data associated with this study are present in the paper or the Supplementary Materials. The RNA-seq data is also available from the corresponding authors upon reasonable request.

Declarations

Ethics approval and consent to participate

This study was fully approved by the National Cancer Center/National Clinical Research Center for Cancer/Cancer Hospital, Chinese Academy of Medical Sciences and Peking Union Medical College (NCC2020A308).

Consent for publication

Not applicable.

Competing interests

The authors declare that they have no competing interests.

Received: 9 March 2022 Accepted: 21 September 2022

Published online: 31 October 2022

References

- Martinez-Quintanilla J, Seah I, Chua M, Shah K. Oncolytic viruses: overcoming translational challenges. *J Clin Invest*. 2019;129(4):1407–18.
- Ribas A, Dummer R, Puzanov I, VanderWalde A, Andtbacka RHI, Michielin O, et al. Oncolytic Virotherapy Promotes Intratumoral T Cell Infiltration and Improves Anti-PD-1 Immunotherapy. *Cell*. 2017;170(6):1109–1119.e10.
- Lichty BD, Breitbach CJ, Stojdl DF, Bell JC. Going viral with cancer immunotherapy. *Nat Rev Cancer*. 2014;14(8):559–67.
- Kroemer G, Galluzzi L, Kepp O, Zitvogel L. Immunogenic cell death in cancer therapy. *Annu Rev Immunol*. 2013;31:51–72.
- Fukuhara H, Ino Y, Todo T. Oncolytic virus therapy: A new era of cancer treatment at dawn. *Cancer Sci*. 2016;107(10):1373–9.
- Harrington K, Freeman DJ, Kelly B, Harper J, Soria JC. Optimizing oncolytic virotherapy in cancer treatment. *Nat Rev Drug Discov*. 2019;18(9):689–706.
- Gujar S, Pol JG, Kroemer G. Heating it up: Oncolytic viruses make tumors 'hot' and suitable for checkpoint blockade immunotherapies. *Oncimmunology*. 2018;7(8):e1442169.
- Shi T, Song X, Wang Y, Liu F, Wei J. Combining Oncolytic Viruses With Cancer Immunotherapy: Establishing a New Generation of Cancer Treatment. *Front Immunol*. 2020;11:683.
- Cook M, Chauhan A. Clinical Application of Oncolytic Viruses: A Systematic Review. *Int J Mol Sci*. 2020;21(20):7505.
- van Vloten JP, Workenhe ST, Wootton SK, Mossman KL, Bridle BW. Critical Interactions between Immunogenic Cancer Cell Death, Oncolytic Viruses, and the Immune System Define the Rational Design of Combination Immunotherapies. *J Immunol*. 2018;200(2):450–8.
- Locati M, Curtale G, Mantovani A. Diversity, Mechanisms, and Significance of Macrophage Plasticity. *Annu Rev Pathol*. 2020;15:123–47.
- Anderson NR, Minutolo NG, Gill S, Klichinsky M. Macrophage-Based Approaches for Cancer Immunotherapy. *Cancer Res*. 2021;81(5):1201–8.
- Logtenberg MEW, Scheeren FA, Schumacher TN. The CD47-SIRPa Immune Checkpoint. *Immunity*. 2020;52(5):742–52.
- Ni H, Cao L, Wu Z, Wang L, Zhou S, Guo X, et al. Combined strategies for effective cancer immunotherapy with a novel anti-CD47 monoclonal antibody. *Cancer Immunol Immunother*. 2022;71(2):353–63.
- Liu J, Xavy S, Mihardja S, Chen S, Sompalli K, Feng D, et al. Targeting macrophage checkpoint inhibitor SIRPa for anticancer therapy. *JCI Insight*. 2020;5(12):e134728.
- Zhang W, Hu X, Liang J, Zhu Y, Zeng B, Feng L, et al. oHSV2 Can Target Murine Colon Carcinoma by Altering the Immune Status of the Tumor Microenvironment and Inducing Antitumor Immunity. *Mol Ther Oncolytics*. 2020;16:158–71.
- Zhang W, Zeng B, Hu X, Zou L, Liang J, Song Y, et al. Oncolytic Herpes Simplex Virus Type 2 Can Effectively Inhibit Colorectal Cancer Liver Metastasis by Modulating the Immune Status in the Tumor Microenvironment and Inducing Specific Antitumor Immunity. *Hum Gene Ther*. 2021;32(3–4):203–15.
- Zhao Q, Zhang W, Ning Z, Zhuang X, Lu H, Liang J, et al. A novel oncolytic herpes simplex virus type 2 has potent anti-tumor activity. *PLoS One*. 2014;9(3):e93103.

19. Wang Y, Zhou X, Wu Z, Hu H, Jin J, Hu Y, et al. Preclinical Safety Evaluation of Oncolytic Herpes Simplex Virus Type 2. *Hum Gene Ther.* 2019;30(5):651–60.
20. Russell-Goldman E, Hornick JL, Qian X, Jo VY. NKX2.2 immunohistochemistry in the distinction of Ewing sarcoma from cytomorphologic mimics: Diagnostic utility and pitfalls. *Cancer Cytopathol.* 2018;126(11):942–9.
21. Guo Z, Zhang X, Zhu H, Zhong N, Luo X, Zhang Y, et al. TEO2 induced progression of colorectal cancer by binding with RICTOR through mTORC2. *Oncol Rep.* 2021;45(2):523–34.
22. Moresco EM, LaVine D, Beutler B. Toll-like receptors. *Curr Biol.* 2011;21(13):R488–93.
23. Shi Z, Cai Z, Sanchez A, Zhang T, Wen S, Wang J, et al. A novel Toll-like receptor that recognizes vesicular stomatitis virus. *J Biol Chem.* 2011;286(6):4517–24.
24. Macedo N, Miller DM, Haq R, Kaufman HL. Clinical landscape of oncolytic virus research in 2020. *J Immunother Cancer.* 2020;8(2):e001486.
25. Bhatt DK, Wekema L, Carvalho Barros LR, Chammas R, Daemen T. A systematic analysis on the clinical safety and efficacy of onco-virotherapy. *Mol Ther Oncolytics.* 2021;23:239–53.
26. Hemminki O, Dos Santos JM, Hemminki A. Oncolytic viruses for cancer immunotherapy. *J Hematol Oncol.* 2020;13(1):84.
27. Lan Q, Xia S, Wang Q, Xu W, Huang H, Jiang S, et al. Development of oncolytic virotherapy: from genetic modification to combination therapy. *Front Med.* 2020;14(2):160–84.
28. Andtbacka RH, Kaufman HL, Collichio F, Amatruda T, Senzer N, Chesney J, et al. Talimogene Laherparepvec Improves Durable Response Rate in Patients With Advanced Melanoma. *J Clin Oncol.* 2015;33(25):2780–8.
29. Zhang B, Huang J, Tang J, Hu S, Luo S, Luo Z, et al. Intratumoral OH2, an oncolytic herpes simplex virus 2, in patients with advanced solid tumors: a multicenter, phase I/II clinical trial. *J Immunother Cancer.* 2021;9(4):e002224.
30. Aurelian L. Oncolytic viruses as immunotherapy: progress and remaining challenges. *Onco Targets Ther.* 2016;9:2627–37.
31. Ricca JM, Oseledchyk A, Walther T, Liu C, Mangarin L, Merghoub T, et al. Pre-existing Immunity to Oncolytic Virus Potentiates Its Immunotherapeutic Efficacy. *Mol Ther.* 2018;26(4):1008–19.
32. Phan M, Watson MF, Alain T, Diallo JS. Oncolytic Viruses on Drugs: Achieving Higher Therapeutic Efficacy. *ACS Infect Dis.* 2018;4(10):1448–67.
33. Malfitano AM, Di Somma S, Iannuzzi CA, Pentimalli F, Portella G. Virotherapy: From single agents to combinatorial treatments. *Biochem Pharmacol.* 2020;177:113986.
34. Kaufman HL, Kohlhapp FJ, Zloza A. Oncolytic viruses: a new class of immunotherapy drugs. *Nat Rev Drug Discov.* 2015;14(9):642–62.
35. Rajani K, Parrish C, Kottke T, Thompson J, Zaidi S, Ilett L, et al. Combination Therapy With Reovirus and Anti-PD-1 Blockade Controls Tumor Growth Through Innate and Adaptive Immune Responses. *Mol Ther.* 2016;24(1):166–74.
36. Mochizuki Y, Tazawa H, Demiya K, Kure M, Kondo H, Komatsubara T, et al. Telomerase-specific oncolytic immunotherapy for promoting efficacy of PD-1 blockade in osteosarcoma. *Cancer Immunol Immunother.* 2021;70(5):1405–17.
37. Mahalingam D, Wilkinson GA, Eng KH, Fields P, Raber P, Moseley JL, et al. Pembrolizumab in Combination with the Oncolytic Virus Pelareorep and Chemotherapy in Patients with Advanced Pancreatic Adenocarcinoma: A Phase Ib Study. *Clin Cancer Res.* 2020;26(1):71–81.
38. Zhu Y, Hu X, Feng L, Yang Z, Zhou L, Duan X, et al. Enhanced Therapeutic Efficacy of a Novel Oncolytic Herpes Simplex Virus Type 2 Encoding an Antibody Against Programmed Cell Death 1. *Mol Ther Oncolytics.* 2019;15:201–13.
39. Meyers DE, Wang AA, Thirukkumaran CM, Morris DG. Current Immunotherapeutic Strategies to Enhance Oncolytic Virotherapy. *Front Oncol.* 2017;7:114.
40. Saha D, Martuza RL, Rabkin SD. Macrophage Polarization Contributes to Glioblastoma Eradication by Combination Immunovirotherapy and Immune Checkpoint Blockade. *Cancer Cell.* 2017;32(2):253–267.e5.
41. Veillette A, Chen J. SIRPa-CD47 Immune Checkpoint Blockade in Anticancer Therapy. *Trends Immunol.* 2018;39(3):173–84.
42. Tian L, Xu B, Teng KY, Song M, Zhu Z, Chen Y, et al. Targeting Fc Receptor-Mediated Effects and the "Don't Eat Me" Signal with an Oncolytic Virus Expressing an Anti-CD47 Antibody to Treat Metastatic Ovarian Cancer. *Clin Cancer Res.* 2022;28(1):201–14.
43. Xu B, Tian L, Chen J, Wang J, Ma R, Dong W, et al. An oncolytic virus expressing a full-length antibody enhances antitumor innate immune response to glioblastoma. *Nat Commun.* 2021;12(1):5908.
44. Huang Y, Lv SQ, Liu PY, Ye ZL, Yang H, Li LF, et al. A SIRPa-Fc fusion protein enhances the antitumor effect of oncolytic adenovirus against ovarian cancer. *Mol Oncol.* 2020;14(3):657–68.
45. Zhao XW, Kuijpers TW, van den Berg TK. Is targeting of CD47-SIRPa enough for treating hematopoietic malignancy? *Blood.* 2012;119(18):4333–4.
46. Yanagita T, Murata Y, Tanaka D, Motegi SI, Arai E, Daniwijaya EW, et al. Anti-SIRPa antibodies as a potential new tool for cancer immunotherapy. *JCI Insight.* 2017;2(1):e89140.
47. Mills CD, Lenz LL, Harris RA. A Breakthrough: Macrophage-Directed Cancer Immunotherapy. *Cancer Res.* 2016;76(3):513–6.
48. Mitchem JB, Brennan DJ, Knolhoff BL, Belt BA, Zhu Y, Sanford DE, et al. Targeting tumor-infiltrating macrophages decreases tumor-initiating cells, relieves immunosuppression, and improves chemotherapeutic responses. *Cancer Res.* 2013;73(3):1128–41.
49. Ruffell B, Chang-Strachan D, Chan V, Rosenbusch A, Ho CM, Pryer N, et al. Macrophage IL-10 blocks CD8+ T cell-dependent responses to chemotherapy by suppressing IL-12 expression in intratumoral dendritic cells. *Cancer Cell.* 2014;26(5):623–37.
50. Rameylte E, Tastanova A, Balázs Z, Ignatova D, Turko P, Menzel U, et al. Oncolytic virotherapy-mediated anti-tumor response: a single-cell perspective. *Cancer Cell.* 2021;39(3):394–406.e4.
51. Wu J, Dobbs N, Yang K, Yan N. Interferon-Independent Activities of Mammalian STING Mediate Antiviral Response and Tumor Immune Evasion. *Immunity.* 2020;53(1):115–126.e5.
52. Yamashiro LH, Wilson SC, Morrison HM, Karalis V, Chung JJ, Chen KJ, et al. Interferon-independent STING signaling promotes resistance to HSV-1 in vivo. *Nat Commun.* 2020;11(1):3382.

Publisher's Note

Springer Nature remains neutral with regard to jurisdictional claims in published maps and institutional affiliations.

Ready to submit your research? Choose BMC and benefit from:

- fast, convenient online submission
- thorough peer review by experienced researchers in your field
- rapid publication on acceptance
- support for research data, including large and complex data types
- gold Open Access which fosters wider collaboration and increased citations
- maximum visibility for your research: over 100M website views per year

At BMC, research is always in progress.

Learn more biomedcentral.com/submissions

